Types of input data

We have benefited of several types of data in order to obtain the thermal emission of a variety Earth-like planets. First, we have used high-resolution thermal emission data of the Earth (Section 3.1), the data are implemented with satellite observations and validated by ground measurements, thus the time series built by the model is an accurate reproduction of an ideally observed light curve of the Earth. Second, we have used global climate model (GCM) simulations (Section 3.2) and by the modification of some specific parameters, we have build the thermal emission of nine Earth-like planets, including the Earth for validation (Section 3.2.1). Finally, we have simulated some of the planets of the previous set by a generic spectral version of the LMD GCM (Section 3.3). Adding the spectral information to the time series, allows us to determine the contribution to the emission, the state and the dynamics of important atmospheric species as carbon dioxide or water vapor. Some of these compounds are called biomarkers as their abundances may indicate the presence of life.

3.1 NASA-SRB Earth data

In Chapter 4, we simulate the thermal emission of the Earth using top-of-the-atmosphere (TOA) all-sky upward longwave (LW) flux maps integrated over the 5-50 μm wavelength interval. The data were obtained from the NASA Langley Research Center Atmospheric Sciences Data Center, they belong to the NASA/GEWEX SRB Project[1] (Suttles et al., 1989; Gupta et al., 1992), whose aim of this project is to determine surface and TOA atmospheric shortwave (SW) and longwave (LW) radiative fluxes with the precision needed to predict transient climate variations and

[1] http://www.gewex.org/

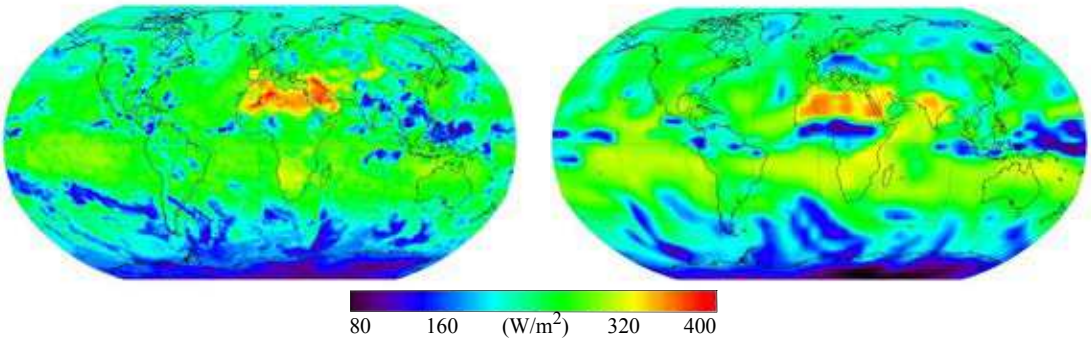

Figure 3.1 Maps of Earth's outgoing mid-infrared radiation. SRB data (left) and LMDZ Earth GCM data (right) at midsummer noon.

decadal-to-centennial climate trends for the Earth.

The GEWEX LW algorithm, uses real measurements to build the emission data (Fu et al., 1997), appliying a thermal infrared radiative transfer code with input parameters derived from the International Satellite Cloud Climatology Project[2] (ISCCP; Rossow et al. (1996), the Goddard EOS Data Assimilation System level-4[3] (GEOS-4), the Total Ozone Mapping Spectrometer[4] (TOMS) archive, and the TIROS Operational Vertical Sounder[5] (TOVS) data set.

An assessment of the quality of the global fluxes was accomplished by comparisons with corresponding ground measurements obtained from the Baseline Surface Radiation Network (BSRN), the Swiss Federal Institute of Technology's Global Energy Balance Archive (GEBA) and NOAA's Climate Montitoring and Diagnostics Laboratory (CMDL). LW flux uncertainties are within ± 5 W/m^2 (σ=1.5%). The data have a time resolution of 3 hr over the whole globe, and a spatial resolution of 1°x1° square cells in latitude and longitude. We used a set that covers a 22 year

[2]http://isccp.giss.nasa.gov/
[3]http://daac.gsfc.nasa.gov/
[4]http://jwocky.gsfc.nasa.gov/
[5]http://www.ozonelayer.noaa.gov/action/tovs.htm

period from 1983 to 2005. A typical map of the outgoing mid-infrared radiation of the Earth, directly represented from the GEWEX data, is shown in Figure 3.5 (left). The map represent the average flux over the period 18:00–21:00 UT for 1 July 2001. It is important to note that in mid-infrared maps, desert zones such as the Sahara-Arabian region appear as warm spots and cold or very humid regions such as clouds over the Antarctica or Indonesia appear as cold spots.

3.2 LMDZ GCM data

In chapters 5 and 6, we use Earth-like planet simulations build with the LMDZ GCM, a Global Climate Model developed by the Laboratoire de Météorologie Dynamique de Paris[6]. The model has 48 grid points regularly spaced in latitude and longitude, yielding a horizontal resolution of 3.75 by 7.5 degrees, and 19 atmospheric pressure levels on the vertical dimension. Sub-grid scale processes such as radiative transfer, clouds, convection, and small-scale turbulence are parameterized as described in Hourdin et al. (2006). The 2-dimensional fields used to compute the thermal emission are output every 3 hours, giving the same time resolution than SRB data. In water-world simulations, the surface is covered by a global ocean – a configuration known as an "aquaplanet" – modeled by a "slab" of a uniform depth of 50 m representing the oceanic surface mixed layer. The evolution of the slab temperature is determined by the surface energy fluxes, as well as heat transport by horizontal diffusion and parameterized wind-driven ocean currents (Codron, 2012). In addition, a simple thermodynamic sea-ice model is used wherever the surface temperature drops below freezing.

3.2.1 Model Validation

With the purpose of validate LMDZ GCM data reproduction of the thermal emission of an Earth-like planet, we have compared the results obtained for the

[6] `http://lmdz.lmd.jussieu.fr/?set_language=en`

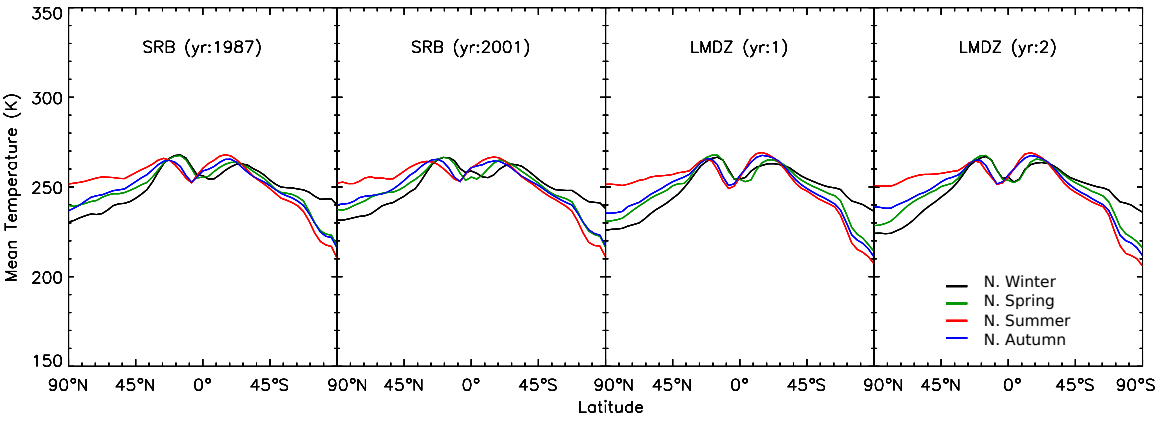

Figure 3.2 Mean Temperature vs latitude, for SRB data (years 1987 and 2001) and LMDZ data (2 years of the sample). Colours represent the position of the planet on the orbit, corresponding to seasons in the northern hemisphere: winter (black), spring (green), summer (red) and autumn (blue).

Earth for both SRB (Chapter 4) and LMDZ GCM (Chapter 5) models. Whereas NASA-GEWEX SRB model is implemented and validated by satellite and ground-based observations, LMDZ calculates the meteorological variables, the transport of numerous constituents (aerosols, chemical compounds of the atmosphere, radio-elements, stable water isotopes, etc...) and benefits from several models to obtain variables such as the vegetation cover, the cycles of water and carbon, the ocean circulation, the marine biochemistry or the dynamics of sea ice.

The main differences between the two models (Fig. 3.1) are the horizontal resolution, which is of 1 by 1 degrees in the case of the SRB model and of 3.75 by 7.5 degrees in the case of the LMDZ model, and the cloud covering. Unfortunately, the representation of clouds in climate models is still unsatisfying. Most cloud properties cannot be resolved by global-scale models and they have to be parameterized in terms of the model variables. Clouds cover the Earth's surface by about 70% and have a very strong effect on the radiation balance of the planet (Section 2.2). Parameterizations are complicated by the fact that clouds cover a large range of scales

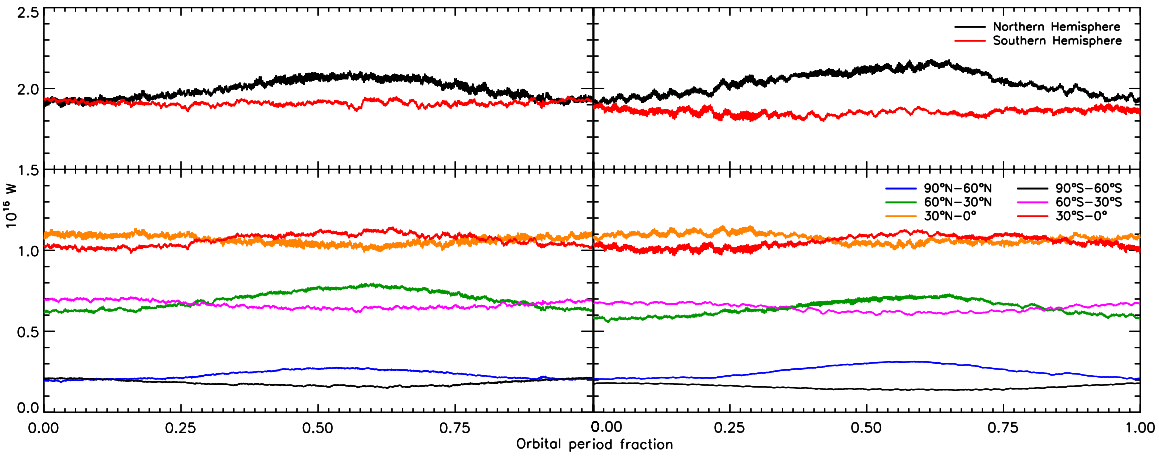

FIGURE 3.3 TOA-flux radiant power of the Earth during one orbit, starting January the 1st, for SRB data (left) and LMDZ data (right). Northern and Southern hemispheres (top) and latitude bands (bottom).

(from microphysics to meso-scale systems), and moreover liquid and ice phases have to be treated separately. Cloud water is predicted by a budget equation where both ice and liquid phases have to be considered jointly. The condensation scheme uses a "hat" probability density function for total water in a grid box, which allows to account for fractional cloudiness, and then the total condensed water is partitioned between liquid water and ice, depending on the local temperature. LMDZ GCM LW cloud radiative forcing has been validated by satellite observations. Doutriaux-Boucher & Quaas (2004) found a discrepancy up to the 40% for mid- and high-latitudes. However, equatorial latitudes, which account for most of the emission, fit to the observations and then global climate parameters are valid.

The mean surface temperature is 288 K in both SRB and LMDZ models, the Bond albedo have a value of 0.31 for SRB-model and of 0.30 for the LMDZ, the effective temperature of the planet is 254 K and 255 K respectively and the normalized greenhouse parameter is 0.39 in both models.

The annual mean brightness temperature per latitude at TOA in both models

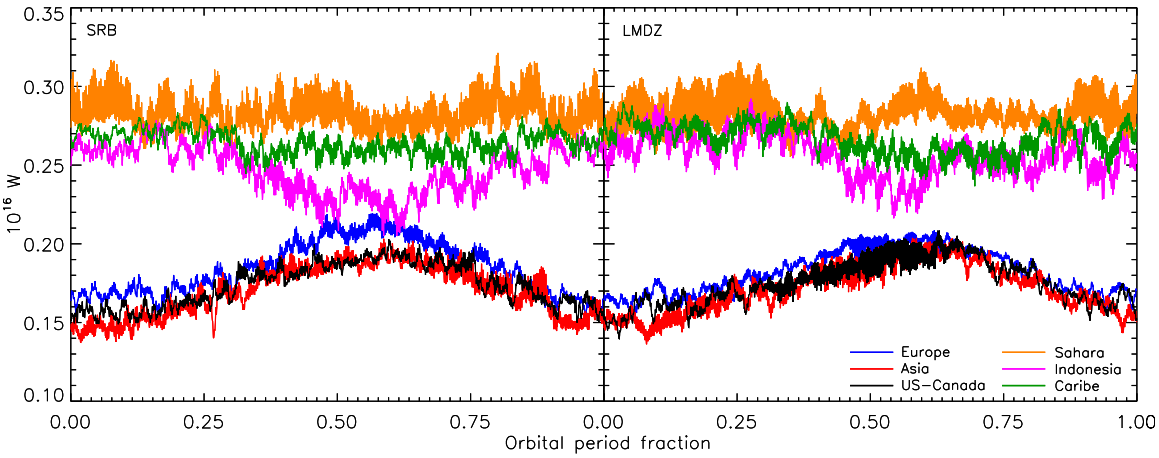

Figure 3.4 TOA-LW radiant power of continental regions of the Northern Hemisphere during one orbit, starting the 1st of January. In the 60°N-30°N latitude band: Europe (blue), Asia (red) and US-Canada (black). In the 30°N-0° latitude band: Sahara-Arabian (orange), Indonesian (magenta) and Caribbean-Mexico area (green). Regions at the same latitude band have equivalent areas.

is also very similar (Fig. 3.2). The profiles show the seasonal variation and the asymmetry between hemispheres: in the Northern Hemisphere, summer and winter are respectively warmer and colder than in the Southern Hemisphere. The prevalence of oceans in the mid-latitudes of the Southern Hemisphere, explains the mild seasonal variation, as water has a low thermal inertia and the temperature does not suffer a great change. Both seasonal and mean temperatures of the poles are similar with slightly colder temperatures in the LMDZ model. The convection clouds assembled at the Intertropical Convergence Zone (ITCZ) have a lower thermal emission at the top than clearer regions, producing the decrease in temperature at the equatorial zone. The seasonal shift of the ITCZ is similar in both models but the central temperature is also colder in the LMDZ. The interannual standard deviation from the mean is around 0.5% in the SRB model, 0.4% in the LMDZ, with 0.7% of variation between the two models.

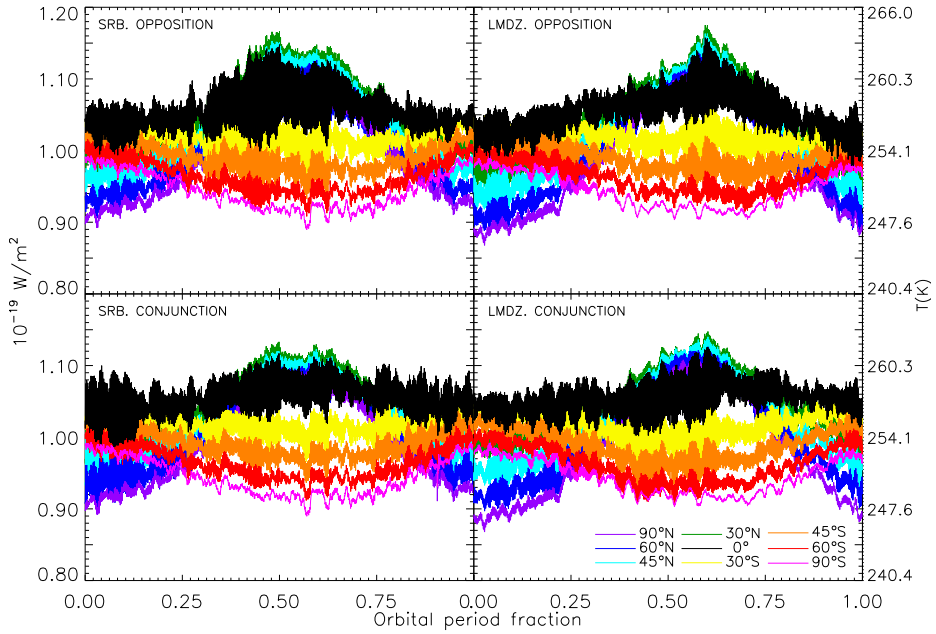

FIGURE 3.5 TOA-all-sky flux towards an observer at opposition (top row) and at conjunction (bottom row) during one rotation for the Earth, SRB data (left) and LMDZ (right) scaled in flux and brightness temperature.Colours indicate the latitude of the sub-observer point.

Once the global parameters are validated, we proceed to check the behavior of the non-averaged emission. We compare the TOA radiant power at different latitudes, with special attention to extreme climate regions, the observed thermal emission for several geometric configurations, the autocorrelation of the series, and the averaged longitudinal curves produced by both models. Figure 3.3 shows the mid-infrared radiant power of the Earth along one orbital period for SRB and LMDZ data respectively. The radiant power is very sensible to the the variability of the emission and contribution of each region to the global mean. We have divided each hemisphere in three latitude-bands: 90°N-60°N (blue), 60°N-30°N (green), 30°N-0° (orange), 90°S-60°S (black), 60°S-30°S (magenta), 30°S-0° (red), and we have computed separately the emission of each hemisphere as long as the emission from the bands.

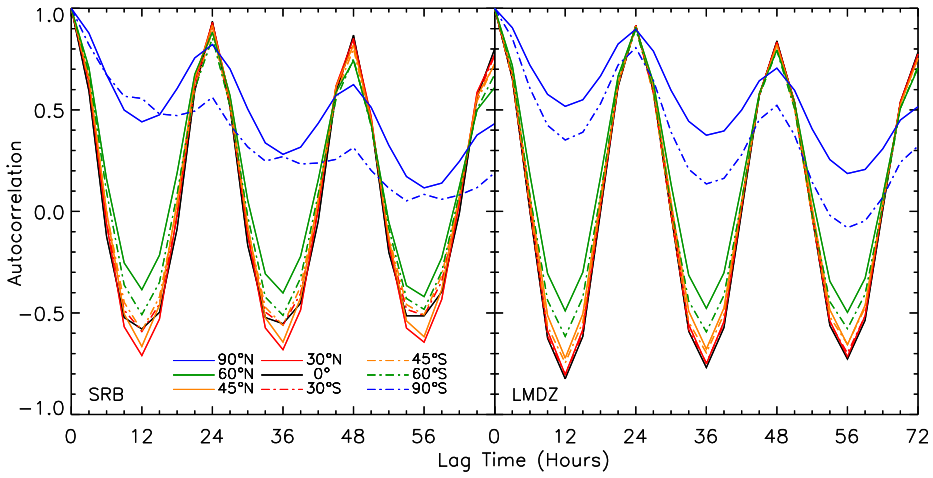

Figure 3.6 Earth autocorrelation at opposition during northern winter for SRB data (left) and LMDZ (right). Colours indicate the latitude of the sub-observer point.

Although the global values are in general in agreement with SRB data, temperatures are slightly colder in the LMDZ, except for the band from 90°N-60°N during summer. As we explain in Chapter 4, tit is interesting to note that the thermal emission of the Earth has a particular characteristic: the Northern Hemisphere emits more radiation than the Southern one (top charts). Comparing both models, the excess during Northern Summer in the LMDZ comes from a warmer Northern Pole during this season. The colder temperatures of the Southern Hemisphere come from a combination of several factors: a higher CRF (specially during the Southern Summer, it appears as a short-frequency variability at equatorial latitudes, Fig. 3.3, red lines) and the colder LMDZ temperatures at the winter poles as the Antarctica (Fig. 3.3, black bottom lines).

Figure 3.4 illustrates the emitted flux along one orbit by certain areas of the planet: Europe, Asia, US-Canada, Sahara-Arabia, Indonesian, and Caribbean-Mexico regions. The short frequency corresponds to the mean temperature variation in the region along the day. This diurnal variability of the signal is modified by the existence

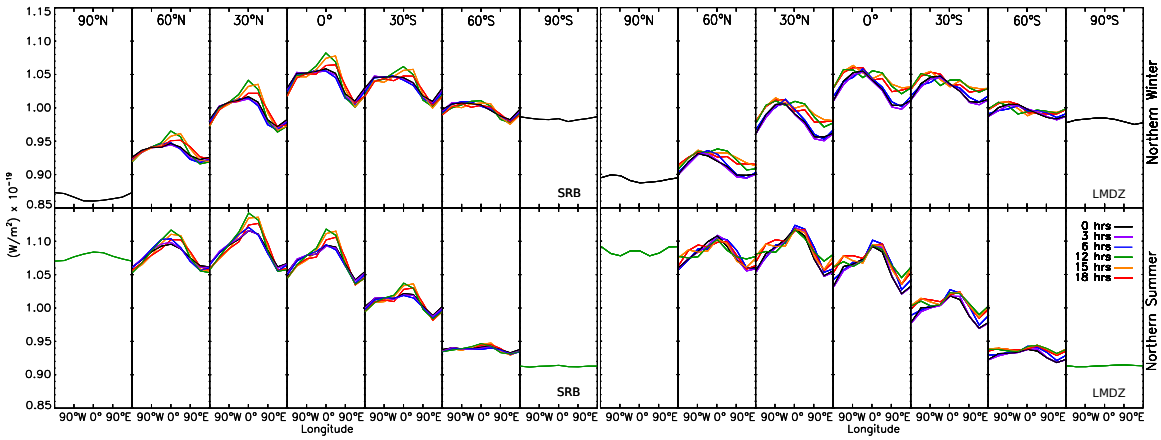

FIGURE 3.7 TOA-all-sky flux Earth rotational curves at opposition during northern winter (top) and northern summer (bottom) for SRB data (left) and LMDZ (right) scaled in flux and brightness temperature. Colours indicate the latitude of the sub-observer point.

of high clouds, the emission coming from the surface is absorbed by the cloud, and then the emission from the cloud top is radiation that actually contributes to the signal. As previously mentioned, in general, temperatures are well reproduced by the LMDZ model but the longwave CRF deviate from the observations. The signal is also less uniform in this case, as the emission shows high values all along Northern Winter with very few perturbations, meaning that the Sahara region is less cloudy during this season. During Northern Summer, a stable cloudy ITCZ appears over the african forest-savanna in LMDZ data (Fig. 3.1, left), as a consequence, the value of the emission from the area considered (0°-30° in latitude) is lower.

Figures 3.5, 3.6, and 3.7 illustrate respectively the TOA thermal emission flux time series, the autocorrelation and the average longitudinal light curves of the Earth in both models. The brightness temperatures, the seasonal cycle and the rotational variability of the time series are well reproduced. The regularity of LMDZ autocorrelation during northern winter is explained by the fact that LMDZ is less cloudy during this season. The deviations in the rotational light curves between the two models are explained by the differences in the cloud treatment and in the

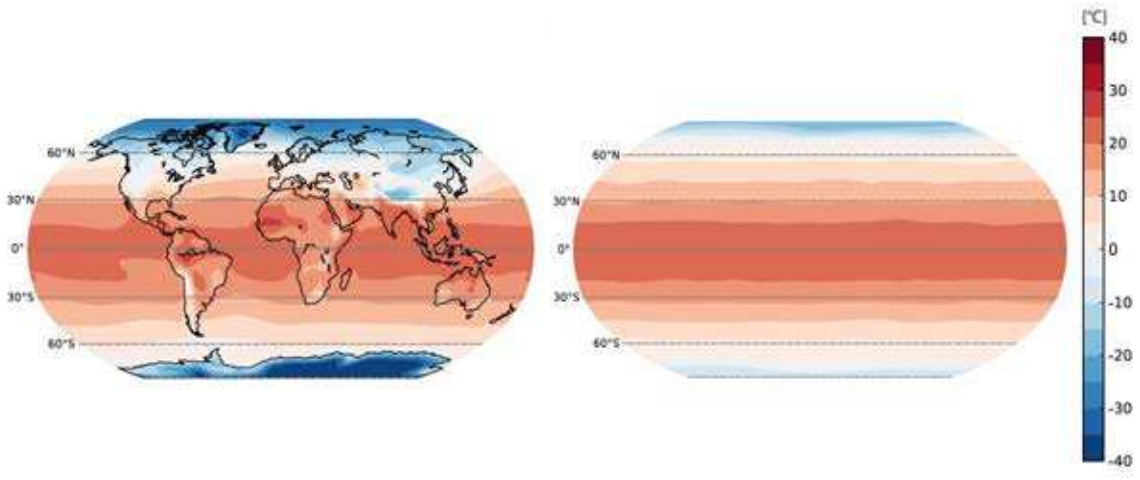

Figure 3.8 LMDZ-generic-GCM surface temperature for the Earth (left) and the aquaplanet O–1 (right) (courtesy of Benjamin Charney, Laboratoire de Météorologie Dynamique, Université P&M Curie (UPMC)).

horizontal resolution. However, the main results are consistent and the deviations that are not critical for this study.

3.2.2 Earth-like planet set

Once we have proven the validity of LMD GCM to reproduce the signal of a terrestrial planet, we obtain the simulations varying one or few parameters at a time, to study the effect on the signal. We have organized our work in two parts:

i) Planets in a terrestrial orbit.– In Chapter 5, we have reproduced the Earth (Ete–1) at first, and then we have built three different planets, keeping the atmospheric composition and the orbital parameters of the Earth and varying the rotation rate and the albedo, in order to study the influence of these two parameters on the climate and the emission. The three planets are: an Earth-like planet with a rotation period of 10 days (Ete–10), an aquaplanet (Ote–1) and a snowball aquaplanet

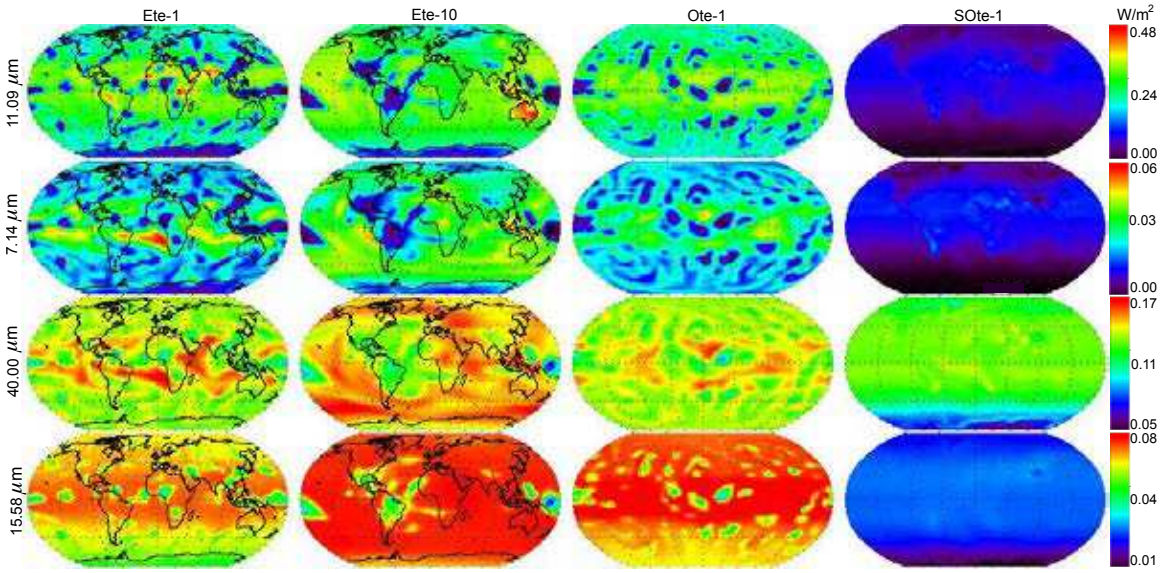

FIGURE 3.9 TOA-flux emission for the bands (from top to bottom): 11.02 μm, 7.14 μm, 40.00 μm, 15.58 μm for the planets (from left to right) Ete–1, Ete–10, Ote–1, SOte–1. The respective wavelength intervals are: (10.63, 11.43) μm, (6.90, 7.41) μm, (35.71, 45.45) μm, and (14.99, 16.21) μm.

(SOte–1) on which the solar constant is diminished to 80% in order to achieve the snowball state.

ii) Water worlds.– In Chapter 6, we study the thermal emission of Earth–like planets covered by a global ocean (aquaplanets). The homogeneous surface of an aquaplanet and the high thermal inertia of water make the rotation rate hard to detect. We have studied five different configurations for a water world. All the planets of the study have the same solar constant as the Earth – with different distance to the star for the synchronous ones– and zero eccentricity and obliquity, to suppress the influence of a seasonal cycle. We have two aquaplanets, named as O–1 and O–10. The first one has a rotation rate of 1 day, and the latter has a rotation rate of 10 days. Then we have build three synchronous aquaplanets, Os–1, Os–10 and Os–360, with rotation rates of 1, 10 and 360 days, respectively. We have compared our results

with those obtained for the Earth and the aquaplanet Ote–1.

3.3 LMD generic GCM spectral data

We have used a new generic version of the LMD Global Climate Model to simulate the spectral light curves of the set of Earth-like planets in a terrestrial orbit (Chapter 5): the Earth, the Earth with a rotation rate of 10 days (Ete–10), the aquaplanet Ote–1 and the snowball aquaplanet SOte–1. This model is derived from the LMDZ Earth GCM (Hourdin et al., 2006), it has been used to study early climates in the solar system (Forget et al., 2012; Wordsworth et al., 2012) and climates on extrasolar planets (Wordsworth et al., 2011; Leconte et al., 2013).

The simulations have a horizontal resolution of 3.75 degrees latitude by 5.625 degrees longitude, a time resolution of 3 hrs and, for comparison with the results obtained from the LMDZ Earth GCM, we have 38 narrowbands with 25 in the broadband of (5-50) μm. In the vertical, the model uses hybrid coordinates, which consist of a terrain-following coordinate system in the lower atmosphere, and pressure levels in the upper atmosphere.

The evolution of the surface temperature is governed by the balance between radiative and sensible heat fluxes, which takes in account the direct solar insolation, the thermal radiation from the atmosphere and the surface, and turbulent and latent heat fluxes, and the thermal conduction in the soil. The parameterization of this last process is based on an 18-layer soil model solving the heat diffusion equation using infinite differences. The depth of the layers were chosen to capture diurnal thermal waves as well as the deeper annual thermal wave. A vertically homogeneous soil is assumed, while the thermal inertia of the ground is set to 2000 $Js^{-1/2}m^{-2}K^{-1}$ everywhere. In equilibrium, the globally averaged difference between outgoing longwave radiation (OLR) and the absorbed solar radiation (ASR) was found to be lower than 2 W/m^2. Simulations for temperate climates are typically

run for 40 years, however as cold climates attain the equilibrium after a longer time, in this model the simulations are run over 80 years to be sure not to miss a full glaciation.

3.4 Summary

To obtain the planetary integrated mid-infrared emission in the direction of a remote observer randomly located, three types of data have been implemented by our model. First we have used satellite validated data from NASA-SRB project in order to obtain an accurate reproduction of the thermal light curve of the Earth (Chapter 4). Secondly, we have used the Earth climate model LMDZ to reproduce the Earth and the results obtained are validated by the comparison with SRB data. Then, we have modeled nine Earth-like planets including: a slow Earth, an aquaplanet and a snowball planet with the orbital parameters of the Earth (Chapter 5), two aquaplanets with circular orbits and three synchronous aquaplanets (Chapter 6). Finally, we present the research possibilities of the multiband LMDZ GCM (Chapter 7).

PART III.

PHOTOMETRIC VARIABILITY OF THE EARTH

Chapter 4

NASA SRB data

We present the analysis of the global-integrated mid-infrared emission flux of the Earth based on data derived from satellite measurements. We have studied the photometric annual, seasonal, and rotational variability of the thermal emission of the Earth to determine which properties can be inferred from the point-like signal. We are interested in the relevant conditions to retrieve the physical characteristics of the planet from the thermal light curve: geography, weather, eccentricity, axis tilt, phase angle, etc. Section 4.1 is an introduction to Earth seen as an exoplanet, the analysis of the time series, rotation rate and longitudinal light curves is presented in Section 4.2. Section 4.5 discuses the contribution of a satellite to the planetary signal and particularly the case of the Earth-Moon system and the conclusions are given in Section 4.6.

4.1 Introduction

Although the aim of numerous studies in transit spectroscopy is the characterization of terrestrial planets around M stars, in this thesis, we are focused in the characterization of an Earth analog around a G star. This case is more challenging for several reasons: G stars are less numerous than M stars, the transit probability in the habitable zone is 10 times lower than it is for M stars, the orbital period (and thus the duration between two transits) is significantly longer for G stars, and the planet-to-star contrast ratio is less favorable for secondary eclipse spectroscopy. For this matter, direct detection seems to be necessary to study Earth analogs around G stars and several instrument concepts have been proposed (Traub et al., 2006; Danchi & Lopez, 2007; Trauger & Traub, 2007; Cash et al., 2009); depending on the concept, it is either the light scattered in the visible or the infrared emission that can be detected. Then, both spectroscopy and photometry can then be used to derive

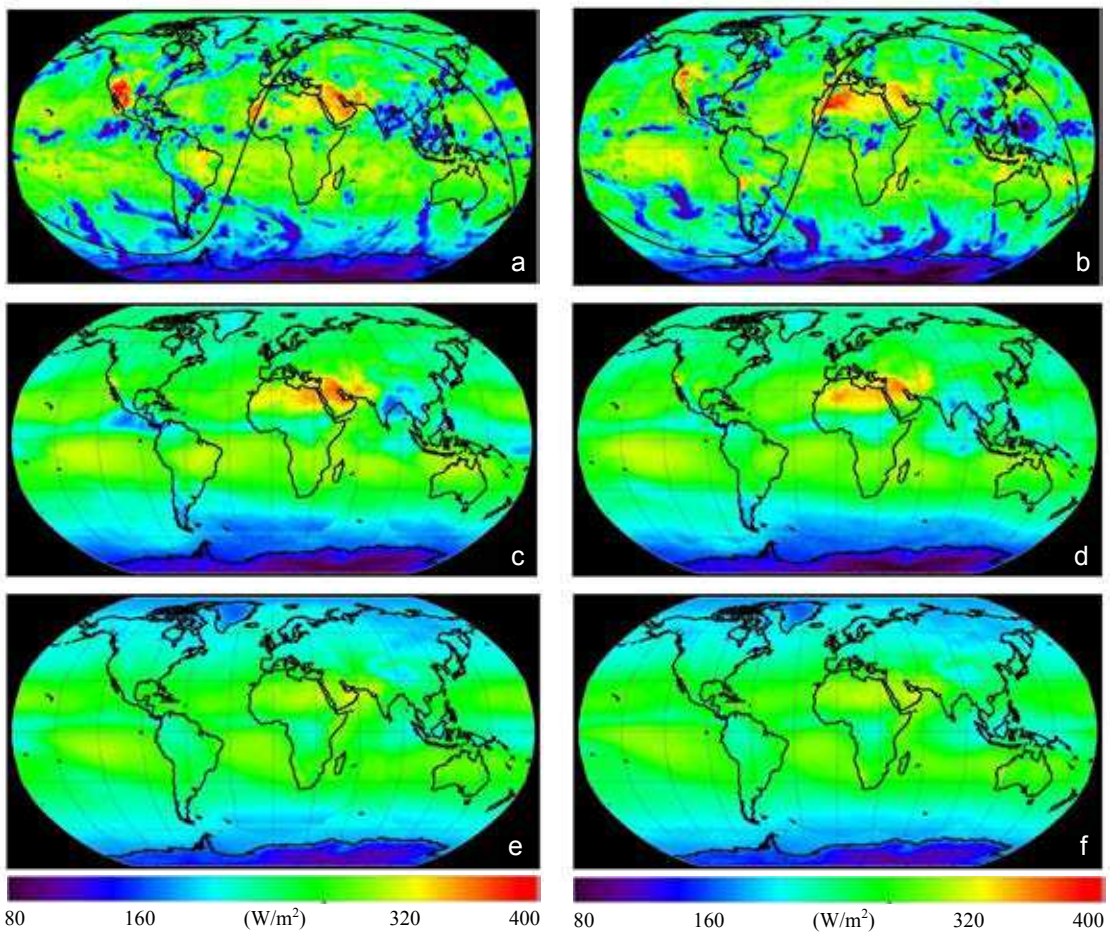

FIGURE 4.1 Maps of Earth's outgoing mid-infrared radiation. Average over the period 18:00–21:00 UT of 1987 July 1 (a) and 2001 July 1 (b) together with the subsolar point and the terminator at the mean time. At that time the brighter regions of the Earth correspond to the deserts of Sahara, Arabian Peninsula, Atacama, and Arizona. Average over the months 1987 July (c) and 2001 July (d). Average over the years 1987 (e) and 2001 (f).

some planetary properties. An important step toward these ambitious programs is to determine what level of characterization could be achieved when observing the Earth as a distant *pale infrared dot*. For instance, in the optical range, broadband photometry can potentially give us information about the albedo and the cloud cover.

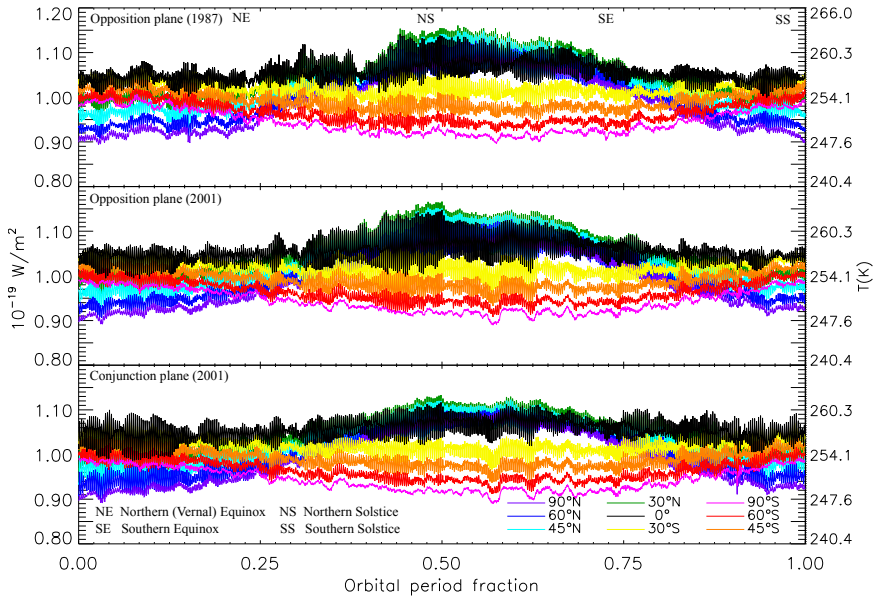

FIGURE 4.2 Time series of the mid-infrared emission flux for the two years of 1987 (top) and 2001 (middle and bottom). The sub-observer's point is represented by the latitudes 90°N, 60°N, 45°N, 30°N, 0°, 30°S, 45°S, 60°S, 90°S, and 0° longitude at the initial time (January 1, 0:00 UT) and the direction planes of opposition (O) (top and middle) and conjunction (C) (bottom).

The uneven distribution of oceans and continents enables the measurement of the 24 hr rotation period by the autocorrelation of the signal for several viewing inclination angles despite the presence of active weather (Pallé et al., 2004, 2008). Visible and near-infrared spectroscopical studies have been made by, e.g., Hearty et al. (2009), Cowan et al. (2011), Robinson et al. (2011), and Livengood et al. (2011) observing rotational and seasonal variations of the Earth spectrum and their influence on the detectability of the spectral signatures of habitability and life.

In this chapter, we provide an integrated mid-infrared (5–50 μm) photometric time series model of the Earth, with 3 hr time resolution, over a period of 22 years of available satellite data. From this geographically resolved data set, we derived the disk-integrated photometric signal of the Earth seen as a point-source planet. The NASA-SRB thermal emission maps of the Earth clearly show warm areas over the